Circus tents, convective thresholds and the non-linear climate response to tropical SSTs

Andrew I. L. Williams[1], Nadir Jeevanjee[2] and Jonah Bloch-Johnson[3]

[1]Atmospheric, Oceanic and Planetary Physics, Department of Physics, University of Oxford, Oxford, UK
[2]Geophysical Fluid Dynamics Laboratory, Princeton, New Jersey, USA
[3]National Centre for Atmospheric Science, Reading, UK

Key Points:

- Contrary to assumptions made in previous work, we find that the climate response to tropical SSTs is highly non-linear.
- These non-linearities are most stark in the Central Pacific, and manifest even for very small perturbation magnitudes.
- Non-linearity is a fundamental consequence of tropical dynamics, with important implications for prior work using linear Green's functions.

Corresponding author: Andrew I. L Williams, `andrew.williams@physics.ox.ac.uk`

Abstract

Using model simulations, we demonstrate that the climate response to localized tropical sea surface temperature (SST) perturbations exhibits numerous non-linearities. Most pronounced is an asymmetry in the response to positive and negative SST perturbations. Additionally, we identify a 'magnitude-dependence' of response on the size of the SST perturbation. We then explain how these non-linearities arise as a robust consequence of convective quasi-equilibrium and weak (but non-zero) temperature gradients in the tropical free-troposphere, which we encapsulate in a 'circus tent' model of the tropical atmosphere. These results demonstrate that the climate response to SST perturbations is fundamentally non-linear, and highlight potential deficiencies in work which has assumed linearity in the response.

Plain Language Summary

Previous work has highlighted that Earth's energy balance is sensitive to the precise distribution of sea-surface temperatures (SSTs), particularly in the tropical Pacific, with important implications for inferring climate sensitivity from the historical record. To quantify this 'SST pattern effect', many studies have adopted a linear framework where the climate response to an SST anomaly is assumed to be a linear function of the sign and size of the anomaly. Here, we show that this assumption is not applicable in many parts of the tropics, particularly the Central Pacific. We classify these non-linearities into two classes and explain why they arise in terms of simple tropical dynamics. To summarize our findings we use a conceptual model of the tropical atmosphere which we term the 'circus tent' model, which represents the dynamics behind these non-linearities in an intuitive way. Our work suggests that previous work which has assumed linearity in the climate response to tropical SSTs may be suffering from compensating biases in their response.

1 Introduction

The spatial pattern of tropical sea-surface temperatures (SSTs) exerts a strong influence on Earth's climate, particularly on the radiative fluxes at the top-of-atmosphere (TOA). First recognized in the context of the El Niño–Southern Oscillation (ENSO) (Bjerknes, 1969; Trenberth et al., 2002; Park & Leovy, 2004), in recent years, this dependence of TOA fluxes on the spatial pattern of SST changes has been re-framed into the broader concept of the 'SST pattern effect' (Stevens et al., 2016). The SST pattern effect has received considerable attention within the community due to its implications for reconciling the anomalously low climate sensitivity inferred from historical energy budget constraints (Otto et al., 2013; Knutti et al., 2017) with the climate sensitivity calculated by equilibrating climate models (Rugenstein et al., 2020; Andrews et al., 2018).

Both modelling (Andrews & Webb, 2018; Zhou et al., 2016; Dong et al., 2019) and observational (Mackie et al., 2021; Fueglistaler, 2019) studies have suggested that the primary mechanism mediating the SST pattern effect is its influence on low clouds in regions of climatological subsidence, and such explanations typically proceed as follows:

- Regions with a high climatological low-cloud amount are generally associated with cold SSTs and a strong inversion (Wood & Bretherton, 2006), thus when SSTs in these regions are warmed the inversion weakens and there is a decrease in low-level cloudiness. This leads to a positive shortwave TOA (SW_{TOA}) anomaly through reduced low-level reflection of incoming solar radiation. The reverse-argument also holds, namely that isolated cooling in these regions strengthens the inversion and increases low-level cloudiness. We term this the 'local stability-inversion' mechanism.

- On the other hand, warming in regions of deep convection is communicated vertically throughout the free-troposphere by deep convection (Y. Zhang & Fueglistaler, 2020) and then horizontally across the tropics through the action of gravity waves (Charney, 1963; Neelin & Held, 1987; Bretherton & Smolarkiewicz, 1989; Pierrehumbert, 1995). This causes a remote warming of the free-troposphere over the aforementioned low-cloud regions which again strengthens the inversion and increases the low-cloud amount. We term this the 'non-local stability-inversion' mechanism.

This explanation has gained significant traction in explaining the SST pattern effect, to the point of appearing in the latest IPCC report (Forster et al., 2021), and is qualitatively supported by analysis of coupled climate model experiments (Ceppi & Gregory, 2017). To put the SST pattern effect on a more quantitative footing some studies have framed the problem in terms of Green's functions (Li & Forest, 2014; Zhou et al., 2017; Dong et al., 2019; Baker et al., 2019) by assuming there exists some operator, $\mathcal{G}$, which maps the spatial pattern of SST anomalies onto TOA anomalies. In this framework, $\mathcal{G}$ can be estimated using ensembles of isolated 'SST patch' experiments in an atmosphere only model and then used to reconstruct the TOA response to arbitrary SST patterns. Although this is an appealing concept, a potential issue is that the Green's function approach is fundamentally linear (Riley et al., 1999) and requires assuming that the TOA response is linear with respect to the sign and magnitude of the imposed SST anomaly, and also that SST anomalies in different regions *combine* linearly. Previous studies have made these assumptions (Barsugli & Sardeshmukh, 2002; Li & Forest, 2014; Zhou et al., 2017; Baker et al., 2019; Dong et al., 2019), but given the well-appreciated 'threshold' behaviour of deep convection (C. Zhang, 1993; Emanuel, 2007; Johnson & Xie, 2010; Xie et al., 2010; I. N. Williams & Pierrehumbert, 2017; Y. Zhang & Fueglistaler, 2020) (see Section 2), along with the observed asymmetry in the atmospheric response to positive and negative ENSO phases (Hoerling et al., 1997, 2001; Johnson & Kosaka, 2016), it seems likely that the linear assumption is not valid.

As such, our goal in this paper is to evaluate the linear assumptions made by previous studies, and to explain why non-linearities arise from the perspective of basic tropical dynamics. We begin by reviewing the theoretical basis for the 'threshold' behaviour of deep convection, and then use atmosphere-only model experiments to show that the TOA response to isolated SST anomalies is in fact non-linear. To explain these findings we then introduce a simple conceptual picture of the tropical atmosphere's response to SST perturbations, which we term the 'circus tent' model, which builds on previous work in the tropical dynamics community. Finally, we show that in regions of deep convection the change in TOA flux associated with a positive SST anomaly can be explained simply by the change in low-level moist static energy and examine to what extent these changes are predictable purely from the SST changes.

2 Theory

To link the dynamics of deep convection to the free-tropospheric temperature profile, we will frequently make use of the moist static energy in this paper, defined as:

$$h = c_p T + L_v q + gz, \tag{1}$$

where c_p is the heat capacity of dry air, T is temperature, g is gravitational acceleration, z is height, L_v is the latent heat of vaporization of water, and q is the water vapour specific humidity. The moist static energy is useful as it is approximately conserved under moist, adiabatic motion.

A central pillar of our understanding of the tropical atmosphere is the assumption of convective quasi-equilibrium (Betts, 1982; Raymond, 1995; Emanuel, 2007), which holds

that deep convection relaxes the free-tropospheric temperature profile to a moist adiabat set by the properties of the subcloud layer. As a moist adiabat is associated with constant saturated moist static energy, this is another way of saying that in regions of deep convection the saturated moist static energy (that is, Eq. 1 but with q replaced by its value at saturation, q^*) of the free-troposphere, h^*_{FT}, should approximately equal the moist static energy of the subcloud layer, h_0.

As mentioned before, gravity waves are efficient at communicating this local temperature profile imposed by convection (or equivalently, h^* profile) across the tropics. This means that deep convection in one region can communicate high values of h^*_{FT} across the local free-troposphere, establishing a 'convective threshold' which inhibit the formation of deep convection if the subcloud h_0 is not sufficient in these regions to overcome the imposed h^*_{FT}.

Using this observation, we follow previous work (e.g., I. N. Williams and Pierrehumbert (2017)) in defining a 'convective instability index', $h_0 - h^*_{500}$, (taking the 500hPa level to be representative of the free-troposphere). In regions unstable to deep convection, we expect this quantity to be positive, whereas in regions stable against deep convection (e.g., subsiding regions) we expect this to be negative and to act as a measure of the inversion strength (similar to Wood and Bretherton (2006), but also accounting for moisture differences as in Koshiro et al. (2022)).
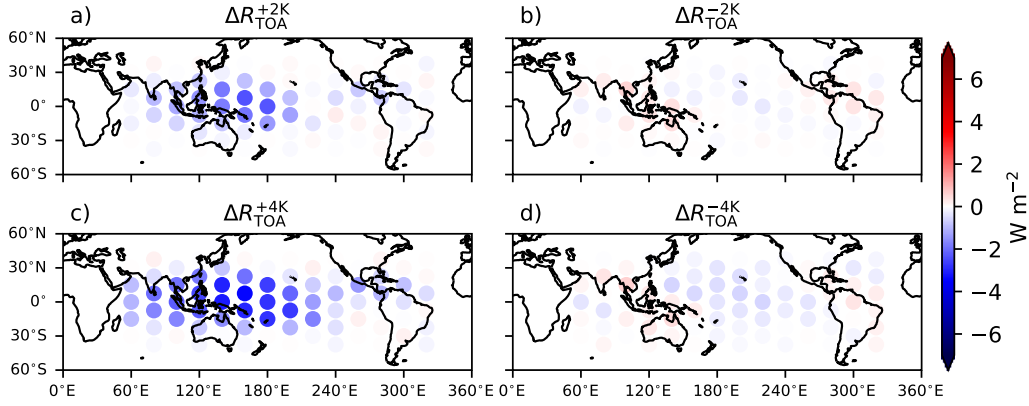
A further simplifying assumption which is frequently made assumption is that h^*_{500} is uniform across the free-troposphere (the 'weak temperature gradient' assumption, WTG), which allows one to replace h^*_{500} with its tropical average value (establishing a single value for the convective threshold). However, as we will show later, this assumption is misleading in the context of the pattern effect, where changes in h^*_{500} are comparable to the variations in baseline h^*_{500} arising from non-zero zonal temperature gradients (Fueglistaler et al., 2009; Bao & Stevens, 2021; Bao et al., 2022). This means that there are actually a spectrum of values for the convective threshold, depending on the local value of h^*_{500}, and to fully understand the pattern effect we cannot assume a single value for h^*_{500}.

3 Methods

We performed a series of atmosphere-only simulations using the ICON (ICOsahedral Non-hydrostatic) general circulation model. The model is run on a triangular grid, at R_2B_4 specification, corresponding to an approximately uniform grid-spacing of 160km on a Cartesian grid. The model uses a terrain-following vertical sigma-height grid with 47 levels between the surface and the model top at 83km. Radiation is parameterized using PSrad scheme (Pincus & Stevens, 2013), and other parameterizations include a bulk mass-flux convection scheme (Tiedtke, 1989), a relative-humidity based cloud cover scheme (Sundqvist et al., 1989) and a single-moment microphysics scheme (Baldauf et al., 2011). In our experiments all greenhouse gases and ozone are fixed at their 1979 levels (A. I. L. Williams et al., 2022).

The control simulation was run for 20 years with a prescribed monthly climatology of SSTs and sea-ice concentrations derived from the Atmospheric Model Intercomparison Project (AMIP) (Neale & Hoskins, 2000) boundary conditions over 1979–2016. Then additional simulations were conducted for 10 years each with an additional 'cosine patch' SST perturbation (following Barsugli and Sardeshmukh (2002)) covering different locations throughout the tropics (locations indicated in Fig. 1). For all simulations, we discard the first year as spin-up and conduct analysis using time-averages over the rest of the simulation period.

The subcloud moist static energy (h_0) was calculated using values at the lowest model level, and the saturated free-tropospheric moist static energy was approximated by its value at 500hPa (h^*_{500}). Our conclusions are insensitive to the precise choice of levels,

Figure 1. Change in global-mean TOA flux (ΔR_{TOA}) associated with each of the SST perturbation experiments. a) Changes for +2K patches. b) Changes for -2K patches. c,d) as in a,b) but for 4K.

and similar results were obtained when either calculating the subcloud moist static energy as the average moist static energy over the lowest 1km (lowest 5 model levels) or calculating the saturated free-tropospheric moist static energy as a bulk average over 700hPa-300hPa. Also note that because h_0 is defined at a given height level, changes in h_0 are only due to changes in temperature and humidity at that level.
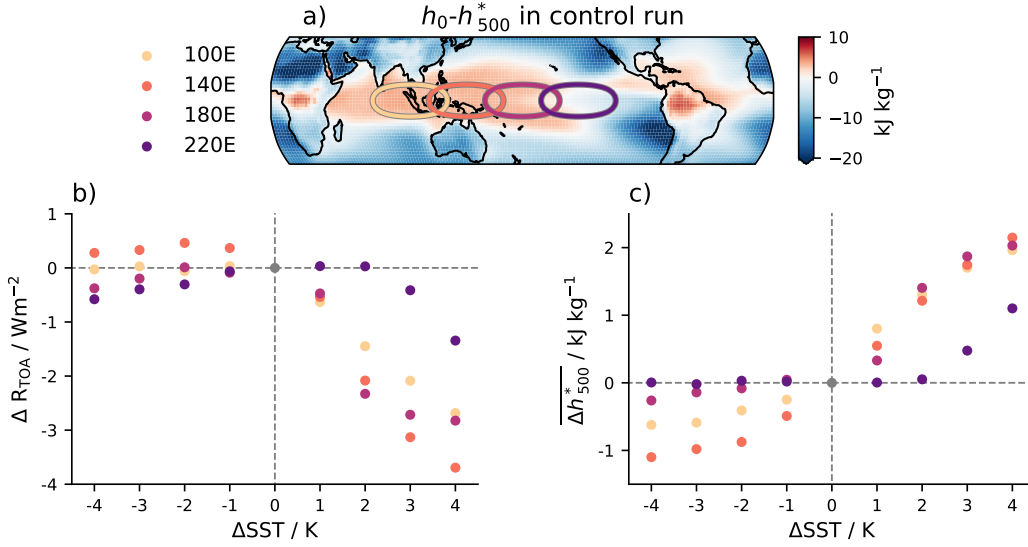
We also define two averaging operators which make the presentation clearer. An overbar $\overline{(\cdot)}$ indicates an average over tropical latitudes ($\pm 30°$), and angle brackets $\langle(\cdot)\rangle$ indicates a 'patch-average' over the region covered by the SST patch perturbation in that experiment (i.e., where $|\Delta SST| > 0$). For sub-cloud changes, the patch-averages exclude land grid-points, and all spatial averages include area-weighting. For example, $\langle\Delta h_0\rangle$ is the change in low-level moist static energy in a particular patch experiment, over all ocean grid-points where $|\Delta SST| > 0$. Similarly, $\langle\Delta h_{500}^*\rangle$ is the change in saturated free-tropospheric moist static energy at 500hPa, over all grid-points where the underlying $|\Delta SST| > 0$ (irrespective of land or ocean).

4 Results

4.1 Non-linearities in the TOA response to tropics SSTs

In Fig. 1 we plot the globally-averaged change in net radiation at the top of the atmosphere (ΔR_{TOA}) for each of the tropical SST perturbation experiments, relative to the control. In agreement with previous work Fig. 1a,c show that warming in the Western tropical Pacific (a region of climatological deep convection), is associated with strong negative changes in the global-mean R_{TOA} flux via the 'non-local stability-inversion' mechanism[1]. Additionally, in subsiding regions the ΔR_{TOA} is slightly positive for the +2K and +4K patches, indicating the 'local stability-inversion' mechanism is at work. However, if we compare these results to the cooling patch experiments in Fig.1b,d we can see there is a marked asymmetry in the ΔR_{TOA} response between the warming and cool-

---

[1] Note that although stability changes over low-cloud regions influence the TOA primarily through SW changes, we use net TOA fluxes to minimize the influence of deep convective clouds, which show up strongly in both the SW and LW but tend to cancel in the net. The results are similar if we focus on the SW (Fig. S1).

Figure 2. a) Set-up for the equatorial sensitivity experiments, overlaid on top of the 'convective instability' parameter (h_0-h_{500}^*) in the control run. b) The changes in global-mean R_{TOA} for each of the sensitivity experiments at $\pm 1K$, $\pm 2K$, $\pm 3K$, $\pm 4K$. c) as in b) but showing the change in tropical-average h_{500}^*, denoted $\overline{\Delta h_{500}^*}$. To account for the varying amounts of land in different patches, in panels b and c the ΔR_{TOA} and $\overline{\Delta h_{500}^*}$ have been divided by the ΔSST weighted land-fraction before plotting.

ing experiments. Notably, whereas warming in convective regions generates a strong negative ΔR_{TOA}, cooling in convective regions only yields a weakly positive ΔR_{TOA} (Fig. 1b), which doesn't increase with further cooling (Fig. 1d). The spatial patterns of ΔR_{TOA} are presented in Fig. S2 for a representative patch in the West Pacific and confirm these findings.

Alongside this 'asymmetry' in the ΔR_{TOA} between warming and cooling patches, there is also another, more subtle, non-linearity that appears in our experiments. To spot this, compare the ΔR_{TOA} responses in the Central Pacific between the +2K experiments in Fig. 1a and +4K experiments in Fig. 1c. Although the ΔR_{TOA}^{+4K} response is generally around twice the ΔR_{TOA}^{+2K} response, in the weakly stable regions of the Central Pacific there are numerous experiments where the ΔR_{TOA} either changes sign or becomes much more negative at +4K compared to +2K. We term this the 'magnitude-dependence' of the SST pattern effect, to convey that the strongly negative ΔR_{TOA} only kicks in for ΔSST above a certain magnitude in these moderately stable regions.

To dig into this more, we have performed additional simulations at $\pm 1K$ and $\pm 3K$ for a subset of four patches along the equatorial Pacific (Fig. 2a). As indicated by the shading in the background of Fig. 2a, these four patches cover distinct convective regimes (as $h_0 - h_{500}^*$ is a measure of convective instability, see Theory). The patches at 100E and 140E are in strongly convective regions (where h_0-$h_{500}^* > 0$), whereas the patch at 220E is in a region which is stable to deep convection (where h_0-$h_{500}^* < 0$) and the patch at 180E is in a transition region. In Fig. 2b we have plotted the global-mean ΔR_{TOA} for each of the four patches at $\Delta SST = \pm 1K$, $\pm 2K$, $\pm 3K$, $\pm 4K$. Again, the asymmetry in the TOA response between positive and negative perturbations is evident. Taking the 140E patch as an example, positive ΔSST perturbations induce a negative ΔR_{TOA} which scales quasi-linearly with the ΔSST magnitude, but for negative ΔSST the TOA

210 response quickly saturates. It is a similar story for the 100E patch, but the signal is weaker
211 for negative ΔSST, however if we subset the TOA response only over subsiding regions
212 we recover the same behaviour (Fig. S3).

213   This asymmetry is also evident in how the ΔSST perturbations impact on the sat-
214 urated moist static energy of the free-troposphere, $\overline{h^*_{500}}$ (Fig. 2c), which makes sense as
215 a higher $\overline{h^*_{500}}$ indicates a warmer and more stable free-troposphere which tends to increase
216 the inversion over low-cloud regions. Looking again at the 140E patch confirms our sus-
217 picion that greater $\overline{\Delta h^*_{500}}$ is associated with greater ΔR$_{TOA}$ for positive values of ΔSST.
218 Conversely, for negative ΔSST there is an initial decrease in $\overline{h^*_{500}}$, which quickly satu-
219 rates. For other 'convective' patch at 100E it is a similar story.

220   Previously we also noted a 'magnitude dependence' of ΔR$_{TOA}$ on the magnitude
221 of positive ΔSST changes in moderately stable regions (Fig. 1a,c) and this is again present
222 in Fig. 2. Looking at the 220E patch results in Fig. 2b, we can see that the sharp de-
223 crease in R$_{TOA}$ does not occur until ΔSST $\gtrsim$ 2K, whereas for the other patches the quasi-
224 linear decrease occurs for all ΔSST $>$ 0K. A similar picture exists for the $\overline{\Delta h^*_{500}}$, which
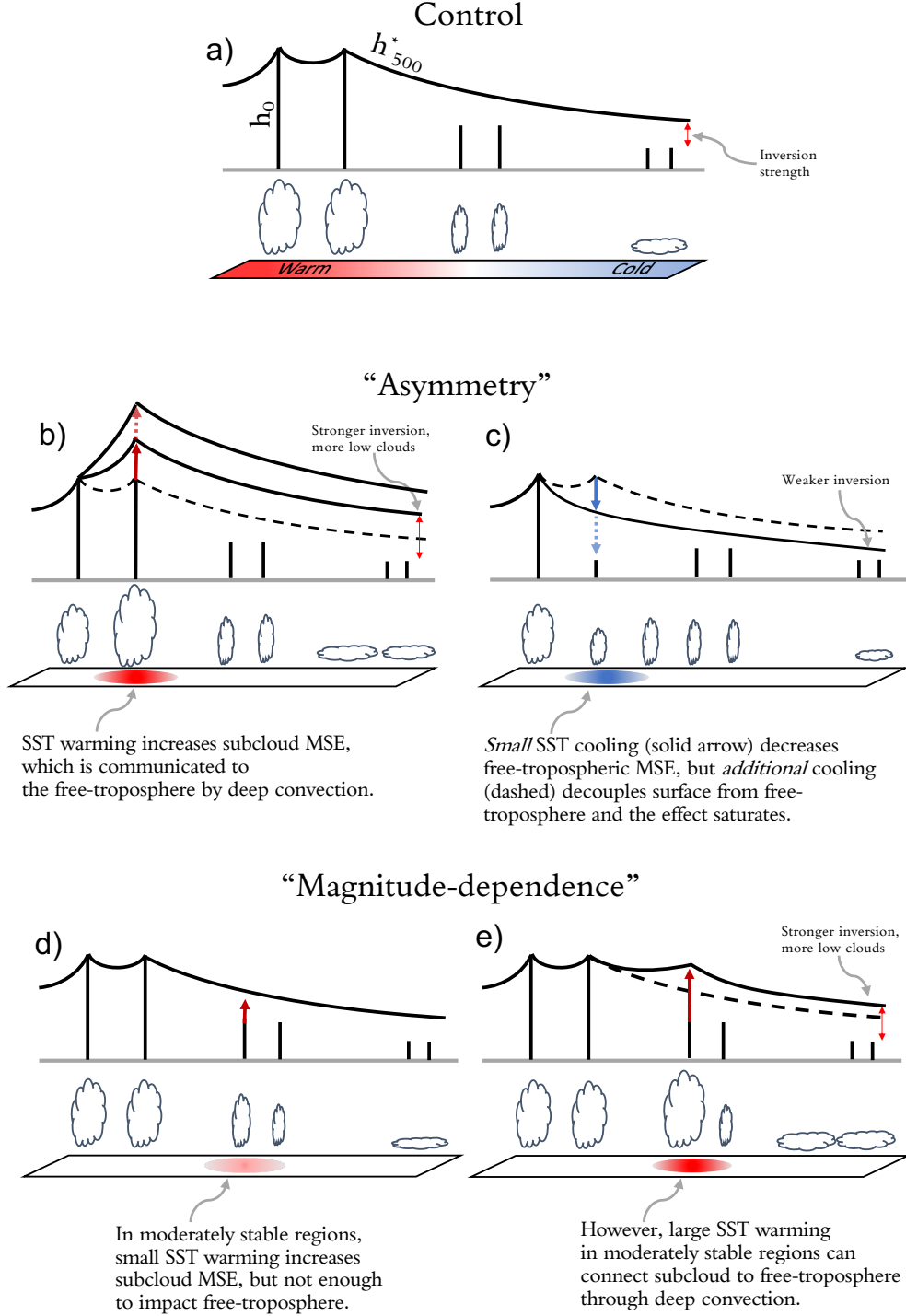225 is unaffected until ΔSST $\gtrsim$ 2K for the 220E patch (Fig. 2c).

4.2 A conceptual for the non-linear response

227   To understand this behaviour, it is helpful to introduce a conceptual picture which
228 builds on our earlier discussion of convective quasi-equilibrium and weak (but non-zero)
229 temperature gradients in the free-troposphere. We call this the 'circus tent' model[2] and
230 it is sketched in Fig. 3a. In this model, the temperature of the tropical free-troposphere
231 (or equivalently, its h^*) can be thought of as being a stiff fabric supported by 'convec-
232 tive tent poles' of different 'heights' corresponding to their subcloud h_0. Where there is
233 deep convection, convective quasi-equilibrium ensures the height of the fabric (h^*_{500}) is
234 roughly equal to h_0, and as one moves away from the convective center the h^*_{500} profile
235 relaxes somewhat until it comes under the influence of a different tent pole. The 'stiff-
236 ness' of the fabric is related to the efficient homogenization of h^* anomalies by gravity
237 waves, and the pattern of Δh^*_{500} appears to be related to the Matsuno-Gill response to
238 tropical heating (e.g., Fig. 1 of Gill (1980)), with an equatorially-confined lobe extend-
239 ing to the East and two off-equatorial maxima slightly to the West of the heating. This
240 pattern can be seen in our maps of Δh^*_{500} (Fig. S4).

241   Using this model we can now understand the impact of warming and cooling in con-
242 vective regions we saw in Fig. 2. The case of positive ΔSST in convective regions is sketched
243 in Fig. 3b. In this case, because the region is already convecting, we are increasing the
244 height of a tent pole which is already 'in contact' with the tent fabric, which raises the
245 h^*_{500} throughout the free-troposphere, including over regions of low-clouds where it strength-
246 ens the inversion. Because the tent fabric is stiff, this also explains why the changes in
247 h^*_{500} and R$_{TOA}$ are approximately linear (Fig. 3b). On the other hand, Fig. 3c illustrates
248 how for negative ΔSST in convective regions the tent pole may be lowered sufficiently
249 to lose contact with the fabric. At this point, further decreases in SST are not commu-
250 nicated to the free-troposphere, which explains the 'saturation' of $\overline{\Delta h^*_{500}}$ and ΔR$_{TOA}$
251 at negative ΔSST (Fig. 2b, Fig. S2, Fig. S5).

252   The circus tent model of the tropics is also useful for understanding the 'magni-
253 tude dependence' we have noted earlier, where even for positive ΔSST, the relationship
254 between ΔSST and $\overline{\Delta h^*_{500}}$ or ΔR$_{TOA}$ can be highly non-linear. This phenomena is most
255 pronounced in moderately stable regions such as the Central Pacific, which correspond
256 to the middle tent poles in Fig. 3a which are not quite tall enough to make contact with

---

[2] This conceptual model was originally suggested by Isaac Held in a 2011 blog post entitled 'Atlantic
Hurricanes and Differential Tropical Warming'.

Figure 3. Schematic representation of the processes controlling the non-linear TOA response to SST perturbations in different convective regimes. a) Illustrates the 'circus tent' model of the tropical atmosphere in the presence of an SST gradient, where deep convection occurs over the warmest SSTs with highest h_0 and is able to perturb the free-tropospheric temperature structure (as measured by h^*_{500}). b) and c) conceptually illustrate how a tropical circus tent responds 'asymmetrically' to warming and cooling in convective regions. d) and e) illustrate how a tropical circus tent responds non-linearly with respect to the magnitude of the SST perturbation in moderately stable regions.

the h_{500}^* fabric (i.e., they sit below the local convective threshold). In this situation, small SST warming raises the subcloud h_0, but may not raise it sufficiently to overcome the convective threshold and make contact with the tent fabric (Fig. 3d). For the SST warming to be able to substantially alter the $\overline{\Delta h_{500}^*}$ or $\Delta \mathrm{R_{TOA}}$, it must be strong enough to raise this tent pole (increase the h_0) enough to make contact with and subsequently raise the height of the tent fabric, as in Fig. 3e. When this condition is met, the local increase in h_{500}^* results in a stronger inversion over low-cloud regions due to the stiffness of the fabric. This explains the sudden decrease in $\Delta \mathrm{R_{TOA}}$ for the 220E patch at $\Delta \mathrm{SST} > 2\mathrm{K}$.

4.3 A linear model for the TOA response to positive ΔSST changes in convective regions

Given the non-linearities we have highlighted in the previous section, a natural question is: "Why do previous Green's function methods still work at all?". One possibility is that the regions of strongest sensitivity in Green's function studies tends to be strongly convective, such as the West Pacific (Dong et al., 2019). Our own analysis shows that the relationship between TOA and $\Delta \mathrm{SST}$ is reasonably linear in convective regions (e.g., compare Fig. 2b and Fig. 2c), and in this section we explore this link in more detail. To do this, in Fig. 4a we first plot the change in patch-averaged h_0 against the patch-averaged changes in h_{500}^* for positive $\Delta \mathrm{SST}$ changes[3]. This acts as a test of the convective quasi-equilibrium hypothesis mentioned earlier, and confirms that changes in subcloud h_0 are efficiently transported into the local free-troposphere in regions of deep convection. Next, in Fig. 4b we check to what extent these local changes in h_{500}^* relate to broader changes across the tropics. In the limit of zero horizontal temperature gradients (perfect WTG) the points in Fig. 4b would lie on the one-to-one line, but we actually find that they lie on a line of constant, but shallower, slope. The shallow slope indicates that the changes in h_{500}^* are not spread uniformly across the tropics (motivating our conceptual model which includes horizontal h^* gradients), and the fact that the slope is constant with increasing local forcing indicates that the fabric of the free-troposphere is indeed 'stiff' as opposed to 'stretchy' (if it was stretchy, we would expect the points to level off at sufficiently high $\langle \Delta \mathrm{h_{500}^*} \rangle$). To confirm the role the changes in h_{500}^* play in the 'non-local stability-inversion' mechanism, in Fig. 4c we scatter the changes in $\overline{\mathrm{h_{500}^*}}$ against $\Delta \mathrm{R_{TOA}}$ and the strong linear relationship indicates that larger changes in free-tropospheric temperature do indeed alter the inversion strength and TOA radiation. Taken together, these results suggest that $\Delta \mathrm{R_{TOA}}$ should be linearly related to the Δh_0 in regions of deep convection, which we find holds reasonable well in our experiments (Fig. 4d).
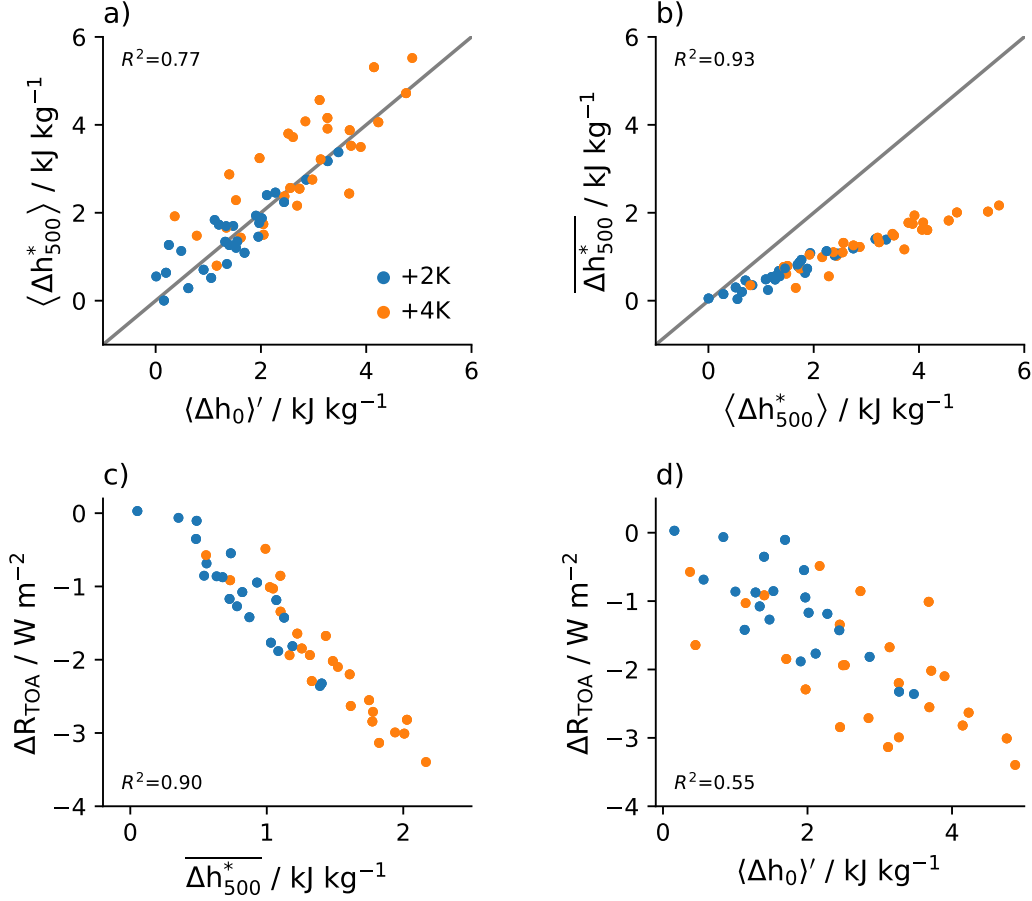
Since local Δh_0 accounts for much of the scatter in $\Delta \mathrm{R_{TOA}}$ for positive $\Delta \mathrm{SST}$ in convecting regions (Fig. 4d), a natural question is: can we relate Δh_0 to the $\Delta \mathrm{SST}$ perturbation more directly? As we defined the subcloud moist static energy at a given geopotential height, we can write the changes in patch-averaged h_0 as :

$$\langle \Delta h_0 \rangle = \langle c_p \Delta T_0 + L_v \Delta q_0 \rangle .$$

Writing $q_0 = \mathrm{RH}\, q_0^*$ and linearizing, we can further approximate this as:

$$\langle \Delta h_0 \rangle \approx \left\langle \left(c_p + L_v \mathrm{RH}_0 \frac{dq^*}{dT} \right) \Delta T_0 + L_v q_0^* \Delta \mathrm{RH} \right\rangle .$$

---

[3] Note that for all of the analysis in Fig. 4, we have only plotted experiments where the patches are locally 'convecting' (i.e., $\langle h_0 \rangle > \langle h_{500}^* \rangle$) either in the control run or in the perturbed run. For the case where the patch 'convects' in the perturbed run but not the control (indicating a situation as in Fig. 3e), we subtract the absolute value of $\langle h_0 - h_{500}^* \rangle$ from the calculated $\langle \Delta h_0 \rangle$ and denote this by $\langle \Delta h_0 \rangle'$ to adjust for the fact that the tent fabric only 'feels' the amount by which the convective threshold is exceeded.

Figure 4. Evaluating the canonical model of the SST pattern effect for warming in convective regions. a) shows a scatter plot of $\langle\Delta h_0\rangle'$ vs $\langle\Delta h_{500}^*\rangle$, as a test of convective quasi-equilibrium. $\langle\Delta h_0\rangle'$ is equal to $\langle\Delta h_0\rangle$ except for if that local patch region does not 'convect' in the control climate (i.e., $\langle h_0\rangle < \langle h_{500}^*\rangle$), in which case we subtract the absolute value of $\langle h_0 - h_{500}^*\rangle$ to adjust for the fact that the tent fabric only 'feels' the amount by which the convective threshold is exceeded. b) shows a scatter plot of $\langle\Delta h_{500}^*\rangle$ vs $\overline{\Delta h_{500}^*}$, as a test of WTG. c) shows $\overline{\Delta h_{500}^*}$ vs the global-mean ΔR_{TOA}, with the strong correlation indicating support for the 'non-local stability-inversion' mechanism. Finally, d) shows a scatter plot of the global-mean ΔR_{TOA} vs $\langle\Delta h_0\rangle'$. Numbers indicate the Pearson coefficient of determination, R^2.

If we also assume Clausius-Clapeyron scaling of q^* $\left(\text{i.e., } \frac{dq^*}{dT} = \frac{L_v q^*}{R_v T^2}\right)$, we arrive at:

$$\langle\Delta h_0\rangle \approx \left\langle \left(c_p + \frac{\text{RH}_0 L_v^2}{R_v^2 T_0^2}q_0^*\right)\Delta T_0 + L_v q_0^* \Delta\text{RH}\right\rangle. \qquad (2)$$
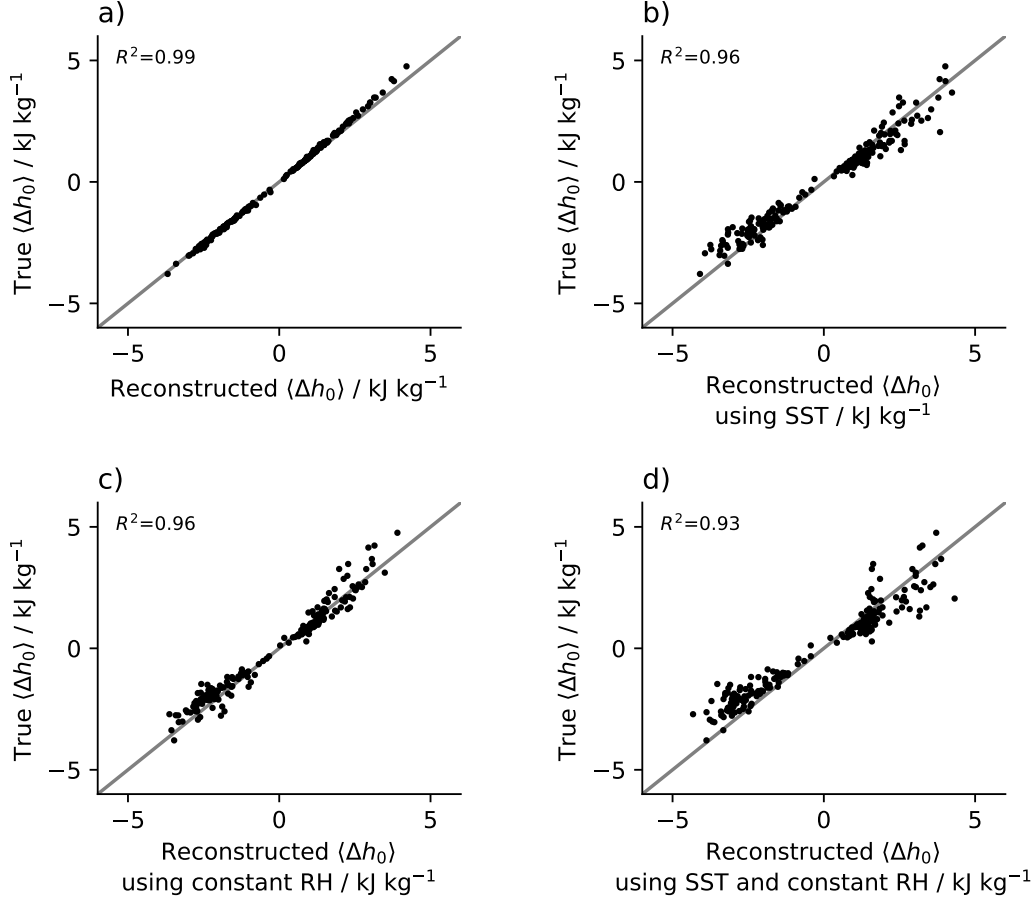
In Fig. 5a, we show that Eq. 2 can capture most of the variations in $\langle\Delta h_0\rangle$ for our patch experiments, although there are slight errors at large, positive ΔSSTdue to the assumption of linearity. If we assume the surface temperature is perfectly communicated across the sub-cloud layer, we can replace $T_0 = \text{SST}$, which also reproduces the modeled $\langle\Delta h_0\rangle$ well (Fig. 5b), with a slight overestimate at higher $\langle\Delta h_0\rangle$. We get similar levels of skill if we assume constant relative humidity but include ΔT_0 (Fig. 5c). This is

Figure 5. Estimating the true $\langle \Delta h_0 \rangle$ in each of the SST patch experiments using: a) Eq. 2. b) Eq. 2 with ΔT_0 replaced by ΔSST. c) Eq. 2 with ΔRH=0. d) Eq. 2 after making both approximations. Numbers indicate the Pearson coefficient of determination, R^2.

equivalent to assuming no changes in moisture convergence into the convecting region (i.e. a purely 'thermodynamic' scaling), which also becomes less valid at strong, positive forcing. Finally, if we combine both of these approximations (ΔRH $= 0$ and $T_0 =$ SST in Eq. 2) we can still reconstruct changes in subcloud h_0 reasonably well (Fig. 5d), even though we are only using information about the SST distribution. This provides support for work which has used SST as a proxy for changes in h_0, however for +4K perturbations we only achieve $R^2 = 0.49$ in this case, which suggests caution should be taken when using SST as a proxy for subcloud MSE at large, positive ΔSST.

5 Discussion and Conclusions

In this work we have shown that the climate response to isolated tropical SST perturbations exhibits strong non-linearities with respect to their sign, magnitude and location. We argue that these non-linearities arise primarily due to the fact that identical SST perturbations do not necessarily perturb the saturated moist static energy of the tropical free-troposphere equally, which is important for setting the inversion strength over low-cloud regions. For example, in moderately stable regions such as the Central Pacific negative SST anomalies have little impact on the global-mean TOA radiation or

tropical h_{500}^*, and positive SST anomalies only have a strong effect when the ΔSST magnitude exceeds a certain value determined by the local convective threshold.

To understand these results, we have introduced the 'circus tent' model of the tropical atmosphere, which brings together the twin pillars of convective quasi-equilibrium and weak (but non-zero) temperature gradients in the tropical free-troposphere. In this model, local ΔSST perturbations only alter the h_{500}^* if the subcloud h_0 exceeds a local 'convective threshold', and then proceeds to perturb the h_{500}^* quasi-linearly for positive perturbations. Negative ΔSST can also decrease the h_{500}^* (Fig. 2c), generating positive ΔR_{TOA} as a result of low-cloud changes, however the effect saturates for sufficiently negative ΔSST because eventually the subcloud layer becomes decoupled from the free-troposphere (Fig. 2b, Fig. 3c). These concepts are understood implicitly in the tropical dynamics community (Zhao et al., 2009; Fueglistaler et al., 2009; Flannaghan et al., 2014; Fueglistaler et al., 2015), but to our knowledge this is the first time they have been *explicitly* invoked to understand the pattern effect.

Our work has implications for studies which construct SST Green's functions by demonstrating that the TOA response is not always linear in ΔSST, even for a given sign, and that the character of the non-linearity varies depending on the convective regime being perturbed. Preliminary work as part of the Green's Function Model Intercomparison Project (GFMIP, Bloch-Johnson et al., 2022, in prep) has also demonstrated similar non-linearities in five other GCMs, suggesting our results are not model-specific. This does not mean the Green's function approach is without merit, but suggests that future work should focus on mapping the TOA response across multiple ΔSST values for each location and understanding the responses in isolation before combining them so as to minimize the risk of introducing compensating errors. This is currently being undertaken in a multi-model context as part of the GFMIP project (Bloch-Johnson et al., 2022, in prep). A particular focus of future work should be on understanding how SST perturbations alter the distribution of subcloud moist static energy, particular over the perturbed region, and understanding what factors set the shape of the tropical 'circus tent' and its response to forcing.

Finally, our work has focused on the climate response to *isolated* SST perturbations and we have not addressed whether these isolated SST perturbations combine in an additive or non-additivity way. Dong et al., (2019) show that when simultaneously perturbing the East and Western Pacific, the response is linear, however our results suggest that this is a fortuitous outcome of perturbing one region already 'in contact' with the tent fabric, and another which sits well-below it (Fig. 3a). Indeed, preliminary experiments as part of GFMIP have shown that non-linearities are stark when simultaneously perturbing two convecting regions, and understanding this non-*additivity* will be the subject of a future paper.

6 Open Research

The climate model simulations in this study are freely available at doi.org/10.5281/zenodo.7139180.

Acknowledgments

References

Andrews, T., Gregory, J. M., Paynter, D., Silvers, L. G., Zhou, C., Mauritsen, T., . . . Titchner, H. (2018). Accounting for changing temperature patterns increases historical estimates of climate sensitivity. *Geophysical Research Letters*, *45*(16), 8490–8499.

Andrews, T., & Webb, M. J. (2018). The dependence of global cloud and lapse rate feedbacks on the spatial structure of tropical pacific warming. *Journal of Climate*, *31*(2), 641–654.

Baker, H. S., Woollings, T., Forest, C. E., & Allen, M. R. (2019). The linear sensitivity of the north atlantic oscillation and eddy-driven jet to ssts. *Journal of Climate*, *32*(19), 6491–6511.

Baldauf, M., Seifert, A., Förstner, J., Majewski, D., Raschendorfer, M., & Reinhardt, T. (2011). Operational convective-scale numerical weather prediction with the cosmo model: Description and sensitivities. *Monthly Weather Review*, *139*(12), 3887–3905.

Bao, J., Dixit, V., & Sherwood, S. C. (2022). Zonal temperature gradients in the tropical free troposphere. *Journal of Climate*, 1–28.

Bao, J., & Stevens, B. (2021). The elements of the thermodynamic structure of the tropical atmosphere. *Journal of the Meteorological Society of Japan. Ser. II*.

Barsugli, J. J., & Sardeshmukh, P. D. (2002). Global atmospheric sensitivity to tropical sst anomalies throughout the indo-pacific basin. *Journal of Climate*, *15*(23), 3427–3442.

Betts, A. K. (1982). Saturation point analysis of moist convective overturning. *Journal of the Atmospheric Sciences*, *39*(7), 1484–1505.

Bjerknes, J. (1969). Atmospheric teleconnections from the equatorial pacific. *Monthly weather review*, *97*(3), 163–172.

Bretherton, C. S., & Smolarkiewicz, P. K. (1989). Gravity waves, compensating subsidence and detrainment around cumulus clouds. *Journal of Atmospheric Sciences*, *46*(6), 740–759.

Ceppi, P., & Gregory, J. M. (2017). Relationship of tropospheric stability to climate sensitivity and earth's observed radiation budget. *Proceedings of the National Academy of Sciences*, *114*(50), 13126–13131.

Charney, J. G. (1963). A note on the large-scale motions in the tropics. *J. Atmos. Sci.*, *20*, 607–609.

Dong, Y., Proistosescu, C., Armour, K. C., & Battisti, D. S. (2019). Attributing historical and future evolution of radiative feedbacks to regional warming patterns using a green's function approach: The preeminence of the western pacific. *Journal of Climate*, *32*(17), 5471–5491.

Emanuel, K. (2007). Quasi-equilibrium dynamics of the tropical atmosphere. *The Global Circulation of the Atmosphere*, *186*, 218.

Flannaghan, T. J., Fueglistaler, S., Held, I. M., Po-Chedley, S., Wyman, B., & Zhao, M. (2014). Tropical temperature trends in atmospheric general circulation model simulations and the impact of uncertainties in observed ssts. *Journal of Geophysical Research: Atmospheres*, *119*(23), 13–327.

Forster, P., Storelvmo, T., Armour, K., Collins, W., Dufresne, J. L., Frame, D., . . . Zhang, H. (2021). The earth's energy budget, climate feedbacks, and climate sensitivity [Book Section]. In V. Masson-Delmotte et al. (Eds.), *Climate change 2021: The physical science basis. contribution of working group i to the sixth assessment report of the intergovernmental panel on climate change* (chap. 7). Cambridge, United Kingdom and New York, NY, USA: Cambridge University Press.

Fueglistaler, S. (2019). Observational evidence for two modes of coupling between sea surface temperatures, tropospheric temperature profile, and shortwave cloud radiative effect in the tropics. *Geophysical Research Letters*, *46*(16), 9890–9898.

Fueglistaler, S., Dessler, A., Dunkerton, T., Folkins, I., Fu, Q., & Mote, P. W. (2009). Tropical tropopause layer. *Reviews of Geophysics*, *47*(1).

Fueglistaler, S., Radley, C., & Held, I. M. (2015). The distribution of precipitation and the spread in tropical upper tropospheric temperature trends in cmip5/amip simulations. *Geophysical Research Letters*, *42*(14), 6000–6007.

Gill, A. E. (1980). Some simple solutions for heat-induced tropical circulation. *Quarterly Journal of the Royal Meteorological Society*, *106*(449), 447–462.

Hoerling, M. P., Kumar, A., & Xu, T. (2001). Robustness of the nonlinear climate response to enso's extreme phases. *Journal of Climate*, *14*(6), 1277–1293.

Hoerling, M. P., Kumar, A., & Zhong, M. (1997). El niño, la niña, and the nonlinearity of their teleconnections. *Journal of Climate*, *10*(8), 1769–1786.

Johnson, N. C., & Kosaka, Y. (2016). The impact of eastern equatorial pacific convection on the diversity of boreal winter el niño teleconnection patterns. *Climate Dynamics*, *47*(12), 3737–3765.

Johnson, N. C., & Xie, S.-P. (2010). Changes in the sea surface temperature threshold for tropical convection. *Nature Geoscience*, *3*(12), 842–845.

Knutti, R., Rugenstein, M. A., & Hegerl, G. C. (2017). Beyond equilibrium climate sensitivity. *Nature Geoscience*, *10*(10), 727–736.

Koshiro, T., Kawai, H., & Noda, A. T. (2022). Estimated cloud-top entrainment index explains positive low-cloud-cover feedback. *Proceedings of the National Academy of Sciences*, *119*(29), e2200635119.

Li, W., & Forest, C. E. (2014). Estimating the sensitivity of the atmospheric teleconnection patterns to sst anomalies using a linear statistical method. *Journal of Climate*, *27*(24), 9065–9081.

Mackie, A., Brindley, H. E., & Palmer, P. I. (2021). Contrasting observed atmospheric responses to tropical sea surface temperature warming patterns. *Journal of Geophysical Research: Atmospheres*, *126*(7), e2020JD033564.

Neale, R. B., & Hoskins, B. J. (2000). A standard test for agcms including their physical parametrizations: I: The proposal. *Atmospheric Science Letters*, *1*(2), 101–107.

Neelin, J. D., & Held, I. M. (1987). Modeling tropical convergence based on the moist static energy budget. *Monthly Weather Review*, *115*(1), 3–12.

Otto, A., Otto, F. E., Boucher, O., Church, J., Hegerl, G., Forster, P. M., . . . others (2013). Energy budget constraints on climate response. *Nature Geoscience*, *6*(6), 415–416.

Park, S., & Leovy, C. B. (2004). Marine low-cloud anomalies associated with enso. *Journal of climate*, *17*(17), 3448–3469.

Pierrehumbert, R. T. (1995). Thermostats, radiator fins, and the local runaway greenhouse. *Journal of the atmospheric sciences*, *52*(10), 1784–1806.

Pincus, R., & Stevens, B. (2013). Paths to accuracy for radiation parameterizations in atmospheric models. *Journal of Advances in Modeling Earth Systems*, *5*(2), 225–233.

Raymond, D. J. (1995). Regulation of moist convection over the west pacific warm pool. *Journal of Atmospheric Sciences*, *52*(22), 3945–3959.

Riley, K. F., Hobson, M. P., & Bence, S. J. (1999). *Mathematical methods for physics and engineering.* American Association of Physics Teachers.

Rugenstein, M., Bloch-Johnson, J., Gregory, J., Andrews, T., Mauritsen, T., Li, C., . . . others (2020). Equilibrium climate sensitivity estimated by equilibrating climate models. *Geophysical Research Letters*, *47*(4), e2019GL083898.

Stevens, B., Sherwood, S. C., Bony, S., & Webb, M. J. (2016). Prospects for narrowing bounds on earth's equilibrium climate sensitivity. *Earth's Future*, *4*(11), 512–522.

Sundqvist, H., Berge, E., & Kristjánsson, J. E. (1989). Condensation and cloud parameterization studies with a mesoscale numerical weather prediction model. *Monthly Weather Review*, *117*(8), 1641–1657.

Tiedtke, M. (1989). A comprehensive mass flux scheme for cumulus parameterization in large-scale models. *Monthly weather review*, *117*(8), 1779–1800.

Trenberth, K. E., Stepaniak, D. P., & Caron, J. M. (2002). Interannual variations in the atmospheric heat budget. *Journal of Geophysical Research: Atmospheres*, *107*(D8), AAC–4.

Williams, A. I. L., Stier, P., Dagan, G., & Watson-Parris, D. (2022). Strong control of effective radiative forcing by the spatial pattern of absorbing aerosol. *Nature Climate Change*, *12*(8), 735–742.

Williams, I. N., & Pierrehumbert, R. T. (2017). Observational evidence against strongly stabilizing tropical cloud feedbacks. *Geophysical Research Letters*, *44*(3), 1503–1510.

Wood, R., & Bretherton, C. S. (2006). On the relationship between stratiform low cloud cover and lower-tropospheric stability. *Journal of climate*, *19*(24), 6425–6432.

Xie, S.-P., Deser, C., Vecchi, G. A., Ma, J., Teng, H., & Wittenberg, A. T. (2010). Global warming pattern formation: Sea surface temperature and rainfall. *Journal of Climate*, *23*(4), 966–986.

Zhang, C. (1993). Large-scale variability of atmospheric deep convection in relation to sea surface temperature in the tropics. *Journal of Climate*, *6*(10), 1898–1913.

Zhang, Y., & Fueglistaler, S. (2020). How tropical convection couples high moist static energy over land and ocean. *Geophysical Research Letters*, *47*(2), e2019GL086387.

Zhao, M., Held, I. M., Lin, S.-J., & Vecchi, G. A. (2009). Simulations of global hurricane climatology, interannual variability, and response to global warming using a 50-km resolution gcm. *Journal of Climate*, *22*(24), 6653–6678.

Zhou, C., Zelinka, M. D., & Klein, S. A. (2016). Impact of decadal cloud variations on the earth's energy budget. *Nature Geoscience*, *9*(12), 871–874.

Zhou, C., Zelinka, M. D., & Klein, S. A. (2017). Analyzing the dependence of global cloud feedback on the spatial pattern of sea surface temperature change with a g reen's function approach. *Journal of Advances in Modeling Earth Systems*, *9*(5), 2174–2189.